2DVD Data Revisited: Multifractal Insights into Cuts of the Spatiotemporal Rainfall Process

Auguste Gires, Ioulia Tchiguirinskaia, D Schertzer, A. Berne

Title: 2DVD data revisited: multifractal insights into cuts of the spatio-temporal rainfall process.

Authors:

Auguste Gires[(1)*], Ioulia Tchiguirinskaia[(1)], Daniel Schertzer[(1)], Alexis Berne[(2)]

(1) U. Paris-Est, Ecole des Ponts ParisTech, LEESU, Marne-la-Vallée, France

(2) Ecole Polytechnique Fédérale de Lausanne, Laboratoire de Télédétection Environnementale, Lausanne, Switzerland

* Corresponding author : auguste.gires@leesu.enpc.fr; +33 1 64 15 36 48 ; Ecole des Ponts ParisTech, LEESU, 6-8 avenue Blaise Pascal, Cité Descartes, Champs sur Marne, 77 455 Marne-La-Vallée Cedex 2

Abstract

Data collected during 4 heavy rainfall events that occurred in Ardèche (France) with the help of a 2D Video-disdrometer are used to investigate the structure of the rain drops distribution in both space and time. A first type of analysis is based on the reconstruction of 36-m height vertical rainfall columns above the measuring device. This reconstruction is obtained with the help of a ballistic hypothesis applied to 1 ms time step series. The corresponding snapshots are analysed with the help of Universal Multifractals. For comparison, a similar analysis is performed on the time series for 1 ms time step, as well as time series of accumulation maps of N consecutive recorded drops (therefore with variable time steps).

It turns out that the drop distribution exhibits a good scaling behaviour on the range 0.5 – 36 m during the heaviest portion of the events, confirming the lack of empirical evidence of the widely used homogenous assumption for drop distribution. For smaller scales

drop positions seems to be homogeneously distributed. The notion of multifractal singularity is well illustrated by the very high resolution time series.

1) Introduction

Rainfall is extremely variable over wide range of scales both in space and time. It has become rather usual to characterize this behaviour with the help of scaling properties, and more recently multifractals (see Lovejoy and Schertzer 1995, Schertzer et al. 2010 for reviews). This framework is physically based in the sense that it is more than a simple tailored statistical framework. Indeed it relies on the cascade process concept which was introduced to reflect the scale invariance properties of the Navier-Stokes equations that govern atmospheric dynamics. It is assumed that the unknown equations governing rainfall inherit these properties of scale invariance (Schertzer and Lovejoy 1987, Hubert et al. 1993). Since the advent of this framework in the 1980s, ample empirical evidence have established its relevancy on scales ranging from few minutes to decades in time and hundreds of meters to planetary size in space (Lovejoy et al. 2008). Some authors reported not a single scaling regime but various ones separated by breaks; typically at few minutes and few days in time and few kilometres in space. Various types of data have been used; rain gauges (de Lima and de Lima 2009, de Lima and Grasman 1999, Fraedrich and Larnder 1993, Ladoy et al. 1993, Olsson 1995, Tessier et al. 1996), disdrometers (de Montera et al. 2009, Gires et al. 2014), weather radars (Gires et al. 2011 2012, Nykanen and Harris 2008, Tessier et al. 1993, Verrier et al. 2010), satellite with TRMM data (Lovejoy et al. 2008) and even numerical outputs of climate simulations (Royer et al. 2008) or meso-scale models (Gires et al. 2011).

The highest resolutions mentioned before are rather coarse with regards to the mm scale down to which atmospheric turbulence - the embedding field of rainfall - is known to exhibit scaling behaviour (see Anselmet et al. 2001 for a review). Hence the need to investigate more precisely the minimum spatio-temporal scales down to which scaling is observed in rainfall fields. Very few studies have analysed this, mainly because of the lack of rainfall data at these scales. Mandapaka et al. (2009) observed on lidar data scaling on the range 1 - 512 s in time and 2.5 - 320 m in space. Lilley et al. (2006) and Lovejoy and Schertzer (2008), using few 3D snapshots of an 8 m^3 volume with most of its drops (Desaulnier-Soucy et al. 2001), reported a scaling behaviour down to few tens of cm with a dependency on the turbulence intensity and drop size. Lovejoy and Schertzer (1990) or Gabbella et al. (2001) using large (~ m) sheets of chemically blotted paper also found a scaling behaviour down to almost drop scale but these results have been disputed (Jameson and Kostinski 1998). In this paper we suggest to investigate more in depth the spatio-temporal (3 dimensions in space and 1 dimension in time) features of rainfall fields down to drop scale using data collected by a 2D video-disdrometer denoted 2DVD hereafter (see Kruger and Krajewski 2002, for a precise description of the device's functioning), deployed in the Ardèche region (South-East of France) in the framework of the HyMeX campaign (Ducrocq et al. 2014), in an innovative way. Indeed this device has been extensively used as a reference in comparison with other rainfall measuring ones (Krajewski et al. 2006, Tokay et al. 2013), or to investigate drops and more generally hydrometeor shape (Battaglia et al. 2010, Cao et al. 2008, Thurai and Bringi 2005) and size (Thurai et al. 2011) distribution features, but not to address this issue of the spatio-temporal structure of rainfall process at drop scale. More precisely vertical, horizontal and temporal cuts of rainfall fields are either obtained or reconstructed with the data provided by a 2DVD and investigated with the help of multifractal techniques.

A related issue is whether drops are homogeneously distributed in space and time. Scaling laws are incompatible with a homogenous distribution (Poisson statistics), but it remains a debated topic. It has mainly been discussed in time by analysing drop counts over various time steps. Most authors have reported deviations from Poisson statistics also not necessarily attributing them to an underlying scaling behaviour; Kostinski and Jameson (1997) used 1 min drop counts by Joss-Waldvogel disdrometer (1967) to most likely invalidate a Poisson framework during heavy rainfall periods (more than 27 drops / min), and confirmed this with 1 s (corresponding to few meters) counts computed with 15 min of 2DVD data (Jameson and Kostinski 1999), noticing that larger drops are more correlated over longer coherence time. Uijlenhoet et al. (1999) also observed deviations from Poisson statistics with 35 min of 10 s time step disdrometer data (~ 6500 drops), but found that the discrepancies are only due to small drops (with diameter smaller than 1.1 mm) which basically do not influence rain rates or reflectivity which are related to higher order moments of the drop size distribution. At the inter-event scale (4 months of data) Lavergnat and Golé (1998) observed a power law decrease of the duration between the observations of two consecutive drops with a disdrometer, which is incompatible with Poisson statistics. Hence in this paper we suggest to also tackle this issue by systematically comparing (when possible!) our results with those that would have been obtained with homogeneously distributed drops. Such methodology was already employed in Lilley et al. (2006) and Jameson and Kostinski (1998).

The collected data is presented in section 2 along with the basic ideas underlying the multifractal framework. Section 3 describes the analysis of snapshots of reconstructed 36 m high vertical columns of air above the device with all its drops. The high temporal resolution of the measuring device is used in section 4 to study 1 ms time step series (over the 11x11 cm^2 sampling area of the device). Drop accumulation maps (therefore with varying time steps, but for the same sampling area) are analysed in section 5.

2) Data description and multifracal framework

2.1) Data description

The data used in this paper were collected with the help of a 2DVD (Kruger and Krajewski 2002). The 2DVD provides detailed information about the geometry and the fall velocity of the particles falling through its sampling area of about 11x11 cm^2, by means of two perpendicular high-speed line cameras (with a pixel size of about 0.2 mm and a time resolution of about 1ms). From the two reconstructed side views of each raindrop, the shape and equivolume diameter are retrieved (assuming the rain drops are oblate spheroids). The two cameras being shifted in the vertical by about 6.5 mm, the fall velocity of each particle is directly measured. The same raw data will be used to generate three types of representation and analysis in the following sections: vertical reconstructed columns, high resolution time series and small scale accumulation maps. Methods used to obtain each cut of the underlying spatio-temporal rainfall representation are included in separated, dedicated section to facilitate the reading of the paper.

The device was installed in Le Pradel, Ardèche, France (see Fig. 1) during the fall 2012 and 2013 in the framework of the HyMeX project (Ducroq et al., 2014). The considered 2DVD is the low version (with reduced wind disturbance). A number of rainfall events were collected, and the two heaviest ones (in terms of 5-min rain rate) for each fall have been selected for the present study. Their main features are summarized in Tab. 1.

2.2) Multifractal framework

The basic principle of the multifractal framework is briefly reminded. For more details refer to the recent review by Scherter and Lovejoy (2011). Multifractals are used to

characterize and also simulate geophysical fields extremely variable over a wide range of spatio-temporal scales which also exhibit long range correlation. It basically relies on the concept of multiplicative cascades. Let us denote ε_λ such a field at resolution λ (=L/l) defined as the ratio between the outer scale L of the phenomenon and the observation scale l. The field at a given resolution λ is obtained from the field at the maximum resolution Λ by averaging it over pixels of resolution λ.

Let us first introduce in a rather intuitive (but less rigorous mathematically) way the notion of multifractal fields with the help of the concept of fractal dimension. A is a geometrical set embedded in a space of dimension d (for instance d = 1 for time series and d = 2 for maps) and N_λ the number of non overlapping d-dimension boxes of size l needed to cover A at resolution λ (= L/l, where L is the outer scale). If the set is fractal then we have:

$$N_\lambda \approx \lambda^{D_F} \qquad (1)$$

where D_F is the fractal dimension of A.

The geometrical set corresponding to the portion of a field ε_λ above a given threshold exhibits fractal features that can be quantified with the help of a fractal dimension. The decreasing dependency of this fractal dimension with regards to the considered threshold reflects the need of multiple fractal dimensions to characterize the field. In a more rigorous mathematical way the threshold is replaced by the scale invariant notion of singularity but the underlying idea remains the same.

More precisely if a field is scaling then its power spectra E is a power-law with respect to the wave number k:

$$E(k) \approx k^{-\beta} \qquad (2)$$

Where β is the spectral slope. A larger β reflects a weaker correlation.

Spectral analysis basically corresponds to a statistical analysis of the moment 2 of the field. In the multifractal framework all the moments are used to fully characterize the variability across scale. The statistical moment of order q at a given resolution scales with the resolution:

$$< \varepsilon_\lambda{}^q > \approx \lambda^{K(q)} \quad (3)$$

Where $K(q)$ is the moment scaling function. In the specific framework of Universal Multifractals (UM), which correspond to the stable and attractive limits of nonlinearly interacting multifractal processes (i.e. a multiplicative generalization of the central limit theorem), $K(q)$ has the following analytical expression :

$$K(q) = \frac{C_1}{\alpha - 1}\left(q^\alpha - q\right) + Hq \quad (4)$$

which only depends on three parameters having a strong physical meaning (Schertzer and Lovejoy 1987 1997):

- H, the degree of non-conservation, which measures the scale dependency of the mean field .H=0 for a conservative field, and can be either positive or negative corresponding to a fractional integration or differentiation respectively of a conserved field;
- C_1, the mean intermittency co-dimension, which measures the mean sparseness of the field, i.e. how concentrated is the mean field. A homogeneous field fills the embedding space and has C_1=0, $0 \le C_1 \le d$ where d is the dimension of the embedding space (a greater C_1 could theoretically exit but it would correspond to fields almost surely null everywhere)
- α ($0 \le \alpha \le 2$), the multifractality index, which measures the variability of the intermittency, i.e. its dependence with respect to the considered level of activity. When α=0, it means that all activity levels exhibit the same intermittency reflecting a fractal field.

The various parameters are related by the following equation from which H is usually estimated:

$$\beta = 1 + 2H - K(2) \qquad (5)$$

3) Analysis of reconstructed vertical rainfall columns

3.1) Ballistic reconstruction of a column

As already explained, the 2DVD provides for each drop a direct measurement of the fall velocity and of the horizontal position within the 11x11 cm^2 sampling area of the device. Assuming the validity of the hypothesis of vertical ballistic trajectories, i.e. that both remain constant during the last seconds of fall and equal to the ones measured near ground surface, it is possible to reconstruct the trajectory of each drop. Achieving this for all the drops enables to reconstruct the whole rainfall field drop by drop on a column above the device (Fig 2.a). The height of the column studied in this paper is 36 m.

The ballistic assumption is extremely coarse. Indeed by assuming an underlying laminar flow, we neglect all interactions with the turbulent wind field and notably shear effects, which have an influence on drops velocity, especially for small ones. Neglecting these effects tend to worsen the quality of the scaling we can observe with the help of this reconstruction. Drop population dynamics (e.g. coalescence in case of collisions, break-ups) is also ignored although wind tunnels studies have shown that raindrop interactions can occur on scales below 36 m (Cotton and Gokhale 1967). Possible effects on the small drop tendency to collide or not, due to small scale turbulence self induced by the aerodynamic forces exerted on the larger falling raindrop (for large raindrops the Reynolds number is of the order of few

thousands) is also not taken into account. However, despite its limitations, this reconstruction can yield some preliminary insight before considering more complex reconstruction, e.g. with randomized trajectories taking into account turbulence effects as well as coalescence and breakup

Finally, the column is divided into 8192 boxes of 4.3 mm height, the two horizontal dimensions being the horizontal sampling area ones' i.e. ~ 11 cm (Fig. 2.b). Although the minimum inter-drop distance (defined as the drop concentration to the power -1/3) observed for the studied events is roughly 4 cm (and usually much larger), the height of the boxes is chosen much smaller so that results can be compared in the vertical and in the horizontal dimension (see section 5). For each box we consider the sum of the p-th power of the volumes V_i of the drops (computed with help of the equivolume diameter D_i estimated by the 2DVD device) contained in this box:

$$\chi_p = \sum V_i^p \qquad (6)$$

As suggested by Lilley et al (2006) by varying p various physical quantities are represented; for instance χ_p for p equal to 0, 1, 7/6 and 2 is respectively proportional to the drop concentration, Liquid Water Content (LWC), rain rate (assuming a fall velocity proportional to the square root of the drop diameter), and radar reflectivity (which is nearly proportional to the 6-th power of the diameter; in the Rayleigh scattering regime). This yields a spatial 1D (vertical) field. An example of vertical evolution of the LWC (basically χ_p for p=1) within the column during the heaviest portion of the 09-24-2012 event is displayed in Fig 2.c. Such reconstructed snapshot of the vertical column above the 2DVD is done every second. Before going on, it should be mentioned that small drops are not fully represented with the 2DVD since measurements for drops with an equivolume diameter smaller than 0.3 mm are unreliable (Tokay et al 2013). It means that small moments are likely to be biased. Nevertheless, the quantities of interest studied in this paper are for p>1 (moment of the

diameter greater than 3) meaning that this limitation does not have a strong influence on the discussed results.

In order to compare the observed properties of the fields with the ones that would be obtained if drops were homogeneously distributed, pseudo-synthetic fields are also generated. To obtain a realization for a given column, the drop centres are re-assigned with the help of a random, uniform distribution, whereas the drop sizes are unchanged. The vertical evolution of the LWC obtained for a realisation is displayed Fig. 2.c.

3.2) Scaling behaviour

Statistical scaling properties are obtained by ensemble averaging (each field sample is first independently upscaled, i.e. its resolution is degraded by averaging over adjacent pixels, then raised to various power *q*, and finally the ensemble average is performed to obtain an estimate of the theoretical moments and its scaling behaviour -Eq. 3-) over 60 consecutive column snapshots (1 min in physical time). The spectral analysis of the field (Eq. 2 in log-log plot) is displayed in Fig. 3.a for the 60 time steps starting on 24 September 2012 at 02:17 UTC with $p = 1$ (i.e. LWC estimate). This is a very intense period of the storm where there are 5573 drops in the column on average (which corresponds to roughly 13 000 drops per m^3) and the rain rate is approximately 180 $mm.h^{-1}$. The rain rate is computed as the average rain rate measured at the level of the 2DVD device (bottom of the column). It is only an indication of the current rainfall intensity since some of the drops present in the studied 60 consecutive snapshots do not reach the device during this minute, meaning that consistent comparison is not possible. We mention it simply because rain rates are much more often used in hydrometeorology than drop concentrations.

The reconstructed fields exhibit a scaling behaviour from 36 m down to roughly 1 m (log k/k_0 ~3 with k_0=1hz). For smaller scales the spectra is flat as it would be for a white noise resulting from randomly homogeneously distributed drops. These findings are confirmed by the Trace Moment (TM) analysis (Eq. 3 in log-log plot) displayed Fig. 3.b for the whole range of available scales and on Fig. 3.c with a zoom on larger scales. It appears that the reconstructed fields exhibit a scaling behaviour (the coefficients of determination r^2 of the linear portions are all greater than 0.99) up to approximately $\lambda = 64$ which corresponds roughly to 0.5 m, a value rather similar to the one found in the spectral analysis. This confirms, on an extended range of scales and using more data, the results of Lilley et al. (2006) who observed scaling from 0.4 m to 2 m on few snapshots of 8 m^3 volume with most of its drops. This suggests that drops are distributed in a scaling manner down to 0.5-1 m and below they are homogeneously distributed, which is in agreement with the findings of Lovejoy and Schertzer (2008).

Similar analyses are also performed on the synthetic fields with homogeneously distributed drop positions. The spectra remains flat on the whole range of scales (Fig 3.d) and the TM analysis curves (solid lines on Fig. 3.b – 3.c) do not exhibit any scaling regime (i.e. linear portion). More quantitatively, over the scaling regime identified for reconstructed fields, the r^2 for the homogeneous fields are typically equal to 0.80. The curves for the smallest scales (roughly 4 mm - few cm) are very similar between reconstructed and homogeneous fields which confirms the results of the spectral analysis for this range of scales. For larger scales, deviations between reconstructed and homogeneous fields are visible with a transition regime before the scaling regime of the reconstructed fields (0.5-36 m). Very similar results are found for other realisations of homogeneously distributed fields showing that these results are statistically meaningful, i.e the Poisson hypothesis of a homogeneous

drop distribution, which is commonly used to model rainfall, is not correct for this minute of the storm. Indeed it does not enable to reproduce the observed structure of drop distributions.

An analysis of the other minutes of this storm and the others lead to qualify this statement. Indeed it appears that a scaling behaviour is retrieved only when there are enough drops in the column (typically more than 2000). To illustrate this, Fig. 4.a displays TM analysis for 60 s starting at 02:23 UTC for the same 09-24-2012 event (415 drops on average in the column, approximately 30 $mm.h^{-1}$). In this case with less numerous drops the linear portions on the TM curves tend to disappear and furthermore the spectra for large scales flattens with β estimates closer to zero, suggesting a behaviour more in agreement with a homogeneous distribution of drops. To get an idea of the number of drops needed in the vertical columns to observe scaling Fig 4.b displays a scatter plot of the r^2 of the TM curve for q=1.5, which is taken as an indication of the quality of the scaling, vs. the average number of drops in the studied vertical columns for the 09-24-2012 event (60 consecutive snapshots are used for each point). Similar plots are obtained for the other events. It appears that scaling is visible only when there are more than 2000-3000 drops in the column, which is the case for roughly 500 snapshots (8 min) during the studied events. In order to get a similar threshold with rain rates, Fig. 4.c displays the rain rate computed vs. the average number of drops in the studied vertical columns for the same minute. The limitations of the comparison between these two quantities are visible on this figure especially for extreme minutes for which the relation is not linear. The indicative rain rate threshold to observe scaling in the vertical columns would be of roughly 75 $mm.h^{-1}$.

For the vertical columns exhibiting a scaling behaviour, we find for scales ranging from 35 m to 0.5 m $\alpha \sim 1.8\text{-}2$, $C_1 \sim 0.005\text{-}0.01$ and $\beta \sim 1 - 1.4$ (slightly smaller than the values found by Lovejoy and Schertzer, 2008). With the help of Eq. 5 it leads to $H \sim 0\text{-}0.2$. H is small enough so that it is relevant to directly implement the TM analysis on the vertical series

297and not on their fluctuations. It is timely to mention that only a limited portion of the scaling
298regime is observed with this data set since there is only a ratio of 64 between the maximum
299and the minimum resolution of the scaling regime. It means that the reliability of the
300multifractal exponent estimates is not very high and their values should not be over-
301interpreted. We will therefore only briefly discuss them. The UM parameter estimates for the
302actual field are slightly different from the ones found by Lilley et al. (2006), with greater α
303and smaller C_1, and the storm to storm variability is also less pronounced but it could be due
304to the fact that here the estimates are discussed only for the most intense portion of the events,
305wheras Lilley et al. performed their analysis only on a limited number of volume snapshots
306from various storms and not necessarily obtained during the peak in rain intensity.

307 The UM parameter estimates are slightly different with especially a C_1 smaller than the
308ones usually reported at coarser resolution ($\alpha \sim 1.7\text{-}1.9$, $C_1 \sim 0.05\text{-}0.2$) by authors who studied
309rainfall field in space (Mandapaka et al. 2009, Verrier et al. 2010, Gires et al. 2013). Although
310these authors studied rainfall fields horizontally which makes direct comparison harder (due
311to a possible anisotropy between the vertical and horizontal directions), this hints at a possible
312break between two scaling regimes, a small scales one and a large scales one, located at few
313tens of meters or few hundreds of meters. Very high resolution data on larger areas would be
314needed to confirm this.

315 The UM estimates are also different from those found for wind turbulence with again
316greater values of α and smaller values of C_1 (Lazarev et al. 1994, Fitton et al. 2011). It would
317mean that there is no trivial link between the drop distributions and the wind turbulence field
318in which they are embedded and from which they presumably inherit the scaling behaviour up
319to a given (high) degree, contrary to the ballistic assumption that was used for the column
320reconstruction and could partially explain the observed differences with wind turbulence

parameters. Development of new instruments providing the size and 3D velocity of each rain drop over few tens of m^3 would be required to properly address this issue.

With the UM parameter estimates found, one can expect sampling limitation and divergence of moment (see Schertzer and Lovejoy 2011 for more details) to affect estimates of $K(q)$ only for q greater than 10, meaning that for lower statistical order the observed scaling is not spurious.

The same analyses were performed with other values of p or only considering drops with an equivolumic diameter D belonging to a given interval. Taking a greater p or only larger drops yields similar results as expected since greater moments enhance the influence of large drops in Eq. 6. There is no significant difference in the scaling for drops up to 2.5 mm (the average number of drops per column remains significant) or p smaller than 3. A tendency of α to decrease and C_1 to increase with larger drops is noticed. For drops with D> 2.5 mm or p>3, the scaling is lost and the discrepancies with the Poisson framework are much less pronounced. An explanation (Lilley et al. 2006) is that large drops decouple from atmospheric turbulence, from which they inherit the scaling behaviour, at a larger scale than small drops. It means that, although the ballistic assumption on the studied scales is likely to be more valid for larger drops, on the limited range of available scales (the maximum range in 35m) it will not be possible to observe scaling behaviour. Another limitation to the study of large drops with this data set is the very low number of drops in the reconstructed columns (typically less than 80 for the period with the heaviest rainfall available) which leads to less reliable statistics.

4) Rain rate time series with 1 ms time steps

4.1) Description of the data

The data provided by the 2DVD enables to compute a rain rate with time steps Δt of 1 ms, given by:

$$R_{1ms} = \frac{\sum_i V_i}{S\Delta t} \qquad (7)$$

Where the sum over the volumes V_i of the drops is now preformed over all the drops that passed through the sampling area S during Δt (1 ms here). Note that we consider a constant sampling area (the maximum one) and do not take into account refinements with regards to edge effects, which can be assumed of second order. This very high resolution rain rate was computed for 35 min (2^{21} time steps) of the 09-24-2012 event and for 140 min (2^{23} time steps) of the other events. The portion with the greatest cumulative depth was selected for each event. Before going on, we should mention that authors are not advocating for the use of 1 ms time step series for routine hydrological applications. Unfortunately, these series are likely to suffer from strong sampling errors, see Frasson et al. 2011 or Jaffrain and Berne 2011 for an illustration of this issue with standard occlusion optical disdrometers having much smaller sampling area. Here we use this series to demonstrate that the mulifractal notion of singularity, mostly perceived at small scales, has also consequences at large scales.

The 1 ms rain rate time series is plotted Fig. 5.b for the 09-24-2012 event along with the same series with 1 s time steps (Fig. 5.c) and the more classical 1 min time step (Fig. 5.d) (i.e. as the average over 60000 consecutive time steps). The temporal evolutions of the number of drops recorded (Fig. 5.a) and of the average mass weighed diameter (Fig. 5.e) per ms is also displayed. Note that due to the high temporal resolution, the “average” is in fact most of the time steps performed over a unique drop. Two striking features should be noted: there are 96 % of zeros while the series was taken from what is commonly considered as a

extreme rainfall event (this percentage ranges from 97 to 99 % for the other events), and the maximum rain rate (over 1ms) is of 60 000 mm/h which is a value much greater than what hydro-meteorologists are used to (this maximum ranges from 30 000 to 60 000 mm/h for the other events). These extremely high rain rates are due to the passing of several drops during the same ms; up to 14 during the 24 September event. Obviously, the diameter of the drops is also important, as it can be seen for the second peak (between minutes 7 and 10) of the event in Fig. 5.c which is not visible on the drop counts time series. From Fig. 5.e it appears that this second peak it is due to larger drops during this period. More standard values of rain rate are retrieved when averaging to the 1 min time steps.

These two features illustrate both the intermittency of the rainfall field and the notion of multifractal singularity, i.e. the fact that the rain rate is not point wise defined because it depends on the time interval over which it is estimated: it usually diverges when considering it for smaller and smaller intervals. Mathematically, it means that the rain accumulation is a singular measure with respect to the usual measure of time (i.e. the one dimensional Lebesgue measure). The need to properly deal with these two complex properties lead to the development of the theoretical framework of multifractals (see Schertzer and Lovejoy 2011 for more details). In this framework the rain rate is expected to behave as:

$$R \approx \lambda^{\gamma} \quad (8)$$

When positive, the singularity γ is the (algebraic) rate of divergence of the rain rate with the resolution. Here the singularity γ corresponding to the maximum peak occurring at about 5 min (Fig. 5) is equal to 0.8, 0.8 and 1.5 for time steps of 1 ms ($\lambda=2.1\ 10^6$), 1 s ($\lambda=2.1\ 10^3$) and 1 min ($\lambda=35$) respectively. The differences are due to the fact that there are several scaling regimes over these scales as will be shown in the next section. In order to emphasize this point on the whole time series, they are also displayed in Fig. 5 in a $\log_\lambda$ scale.

395<u>4.2) Temporal multifractal analysis</u>

396

397 Figure 6 displays the spectral analysis and the TM analysis for the 10-23-2013 event
398for which the total duration taken into account is 140 min enabling to study a 2^{23} length time
399series (of 1 ms rain rates)! Such duration was chosen because it is the longest one enabling to
400remain in the event and to have a series whose length is a power of 2 as it is needed for the
401simplest TM analysis. Similar curves are obtained for the other events. The spectra does not
402reflect a very good scaling behaviour and it seems that there is a scaling breakdown for the
403frequency *k* roughly equal to 70 ($\log(k/k_0) \sim 4.2$ with k_0=1hz), which corresponds to 2 min^{-1}
404(the breakdown is also at roughly 2 min^{-1} for the 09-24-2012 event, the series of which is
405shorter). The coefficient of determination of the linear portion for large scales is weak (equal
406to 0.68), hence the estimates of the spectral slope β are not reliable and will therefore not be
407discussed. No spectral slope can be derived for smaller scales. On the TM analysis three
408scaling regimes can be indentified: 140 min – few min (from 2 to 8 min according the event)
409with a rather good scaling (r^2 = 0.97-0.9) -blue lines in Fig. 6.b- ; a transition regime in the
410range few min – 32 ms with a rather bad scaling -red lines in Fig. 6.b-; and a very small scales
411regime 32 ms – 1 ms with a good scaling (r^2 = 0.99) -green lines in Fig. 6.b-. The poor quality
412of the scaling observed on the spectral analysis means that the results of the TM analysis
413should not be “over-interpreted”. We observe similar scaling regimes to those reported and
414discussed by Schertzer et al. (2012), i.e. the multifractal regime for 1 day – 7 min and the
415fractal regime for 2 s – 1 ms, obtained with the help of a multifractal analysis by
416Tchiguirinskaia et al. (2003) of an infrared optical spectro-pluviometer time series (Salles et
417al. 1998).

418 For the small scales (32 ms – 1ms) we indeed find an index of multifractality α
419roughly equal to zero meaning that the observed behaviour is monofractal. C_1 is in the interval

4200.7 – 0.85 and estimates are roughly equal to the fractal co-dimension of the time series which
421means that this regime simply reflects the passing of individual drops through the sampling
422area. Given the poor quality of the scaling, UM estimates are not computed for the medium
423scales corresponding to the transition regime. With regards to large scales, the UM parameters
424estimates for all the events are reported in Table 2. The values of α are no longer equal to zero
425meaning that an actual multifractal behaviour coming from the common influence of several
426drops is retrieved (contrary to what was observed for small scales). The strong variations
427according to the event are much greater, especially for α, than those expected if various
428realizations of the same process were analysed. It means that the UM parameters seem to
429depend on the event. The standard drop size distribution (DSD, $N(D)$) was computed for each
430event on average (not shown here) and it appears that the observed differences in the UM
431parameters are not related to DSD differences (especially to the thickness of the tail). There is
432for now no clear explanation for the physical process to which the UM parameter estimates
433differences could be attributed, and further investigations would be required to clarify this.
434 In order to be able to compare these results in time with those obtained on the vertical
435column in the previous section; one has to consider similar time scales. According to its size
436the duration taken by a drop to fall through the 36 m vertical column is between few seconds
437and few tens of seconds (observed drop velocity are between 0.5 and 10 $m.s^{-1}$). This range of
438scales corresponds to the middle regime for which there is no clear scaling behaviour. It might
439be due to the fact that the data is considered for the whole event and not only for the most
440intense portions as it is done for the spatial 1D analysis. In order to test this hypothesis a TM
441analysis was carried out considering only on the one minute long time series of the 09-24-
4422012 event. Successive minutes starting every 15 s (moving window) were considered during
443the event and the scaling was quantified on the range 2 s to 33 s which would corresponds to
444the regime observed in the vertical column. It appears that some minutes exhibit good scaling

(with r^2 greater than 0.98) and other no (with r^2 smaller than 0.90) without any direct link with the corresponding rainfall intensities. This confirms the bad scaling observed on this range of scale with longer time series, and invalidates the tested hypothesis. It means that more investigations on the 3+1D structure of rainfall would be needed to properly link the results between the two types of analyses which are furthermore affected by the bias associated with the coarse ballistic assumption in this paper.

5) Rain drop accumulation analysis

5.1) 2D rain drop accumulation for a given number of consecutive drops

The aim of this section is to study the spatial distribution of the accumulation of a given number N of consecutive drops at ground level (more precisely at the height of the 2DVD) over the sampling area of the device (11x11 cm^2). A 634 x 634 matrix corresponding to pixels seen by the 2DVD is created. To compute the pixel by pixel accumulation, the volume of a drop passing through the 2DVD is evenly distributed between all the pixels that are partially or totally obscured (information provided by the 2DVD), hence the unrealistic square shape of drops visible on the related figures. The drop accumulation is obtained by summing the contribution of *N* consecutive drops to yield either a 2D rain accumulation map or a 2D drop occurrence map. Various *N* (from 50 to 2000) were tested and yielded similar results. Finally a 512 x 512 pixels portion (a 9x9 cm^2 area in the middle of the domain which enables to remove potential bias due to instrumental side effects) is extracted to carry out fractal and multifractal analysis. Figure 7 displays an example of a rain drop accumulation of 150 consecutive drops during the 10-23-2013 event. As in section 3, each (natural) drop

accumulation map is compared with a homogenised version, i.e. a synthetic drop accumulation map. This synthetic map is obtained by keeping the same drops with their size and volume, but randomly homogeneously distributing their position over the sampling area with the help of a uniform law. A natural drop accumulation and one of its homogeneous versions are displayed in Fig. 7. Finally the duration needed to record *N* consecutive drops is also retrieved and will be analysed.

5.2) Fractal and multifractal analysis

The box-counting technique (i.e. Eq. 1 in log-log plot) was applied to drop occurrence accumulation maps to determine their fractal dimension. It is first applied to the drop centres, and then to the pixels occluded by drops. Both are displayed in Fig. 8.a and 8.b for the 10-23-2013 event with 150 drops per maps respectively. The numbers of selected pixels $N(\lambda)$ were averaged over the ensemble of 1179 pictures recorded on a total duration of 12 h for each resolution λ (Eq. 1). Very similar results are observed for the 4 other events and therefore not shown here. Fig. 8 displays a plateau for scales smaller than approximately 12 mm ($\lambda \geq 8$), due to the fact that the resolution of pixels is too high with respect to the number of drop centres. For larger scales (23 – 92 mm, $4 \geq \lambda \geq 1$), the box-counting technique yields a fractal dimension 2, meaning that the drop centres are homogeneously distributed and filling the whole embedding space. The disagreement with the result of Lovejoy and Schertzer (1990) who recorded the position of 452 drops on 128 cm x 128 cm chemically treated blotting paper, discussed and finally confirmed by Gabbella et al. (2001) seems to be merely due to the fact that the scale of the sampling area is too small to reach one of the inhomogeneous regimes. This is in agreement with the fact that the rainfall field exhibited a scaling structure down to 0.5 m and a homogeneous distribution for smaller scales (see Sec. 3)

When analysing the pixels occluded by drops and not only the distribution of drop centres, similar features are retrieved for large scales, but for small scales two fractal dimensions are obtained: respectively 1.1 in the range 23 mm – 1 mm ($4 \leq \lambda \leq 128$, red line in Fig. 8.b) and 1.65 for scales smaller than 0.7 mm ($128 \leq \lambda$, green line in Fig. 8.b). This disagreement with the homogeneity of the drop centres might be due to the variability of the rain volumes (due the drops' sizes) that occurs over smaller scales.

A TM analysis was carried out on rain accumulation maps (not shown here). The main results are that the observed scaling is very bad, and that the curves obtained by analysing the random-position pictures are very similar. This is simply a confirmation that there is no clear scaling regime for scales smaller than 9 cm which as already mentioned was expected from the results of section 3.

5.3) Analysis of the distribution of duration needed for each picture

In this section, the durations needed to obtain *N* consecutive drops through the sampling area are analysed. Figure 9.a displays the strong fluctuations of the series of theses durations for the 10-27-2013 event and *N*= 350. The event lasted 9.3 hours with a total number of series of *N* drops equal to 302. Figure 9.b displays the exceedance probability distribution of the durations in a log-log plot, which exhibits a power-law tail (linear slope in the log-log plot). This feature is opposed to Poisson statistics that yield exponential fall-off of the probability distributions. For this event the power-law is visible for scales ranging from 30 s to 10 min. Larger scales are not taken into account since they correspond to inter-event features rather than the intra-event ones which are accessible with the available data set. For a more extensive study on inter-event analysis refer to Lavergnat and Golé (1998) who also observed power-law behaviour in a slightly different context since they considered much

longer time series and N=1. The exponent of the power law is found roughly equal to 0.8-0.9 for N=350 and similar values are found for other N with a slight tendency to decrease with increasing N (N ranging from 50 to 500, with steps of 50, were tested). The same power law behaviour is also observed for the 10-23-2012 event. For the 10-26-2013 and 09-24-2012 events, the range of available durations does not enable to see the power law (especially true for the 09-24-2012 event). For the 10-20-2012, the range of available duration is similar to the one for the 10-27-2013 and 10-23-2013 events but the scaling is not very good as it was already noticed while analysing the 1 ms time series.

6) Conclusion

In this paper 2DVD data of 4 rainfall events were analysed to grasp some insights into the 3+1D structure of the rainfall field at the drop scale. Firstly, based on a ballistic assumption, vertical 36 m high rainfall columns above the measuring device are reconstructed. It appears that during the most intense portions of the events a good scaling behaviour is retrieved on scales ranging from 0.5 m to 36 m. This inner scale seems to depend on the drop size distribution and larger scale data would be needed to investigate more in depth this dependency. These observations are incompatible with a homogeneous distribution of drops. On the other hand for smaller scales the observations are in agreement with the hypothesis of a homogeneous distribution of drops. Results show that integrated values (such as number of drops or LWC) are well represented by UM simulations for heaviest rainfall period on scales ranging from 0.5m to 36m. An interesting future perspective, that would

require more investigations which are beyond the scope of this paper, would be to actually generate a rainfall simulator at drop scale which enables to reproduce observations. This simulator would need to be capable of integrating break-up and coalescence as well as small scale turbulence wind effect in order to overcome the limitations of the ballistic assumption used here. Results show that using a multifractal framework would be relevant, to design this rainfall simulator.

Secondly, 1 ms rain rate time series are analysed. With such resolution it is possible to actually grasp the underlying assumption of the multifractal framework that rainfall is extremely concentrated on small portions of time or space. The mathematical interpretation is that rain accumulation is actually a measure that is singular with respect to the usual space / time measures (Lebesgue measures). Two scaling regimes are confirmed with a transition in between. The first one for very small scales (1 ms – few tens of ms) is actually fractal and corresponds to rather individual drops. The large scale multifractal regime (few min, few tens of min) correspond to a kind of collective regime of drops and UM parameter values depend on the event. We found that multifractality index α ranges between 1 and 2 and the codimension of the mean intermittency C_1 between 0.2 and 0.5.

Thirdly, N consecutive drop accumulation maps observed by the measuring device are analysed. Fractal spatial analyses were carried out on the actual drop accumulation, as well as homogeneised versions. Both yield very similar results and do not exhibit scaling features. This is due to the fact that the size of the sampling area (11 cm x 11 cm) is smaller than the inner scale of the scaling regime identified with the analysis of the vertical columns. Nevertheless, the distribution of the durations needed to record N drops, exhibits a power law tail, which invalidates the usual hypothesis of a Poisson distribution

The spatio-temporal structure of the rainfall field is investigated through the analysis of 1 D (vertical column, time series) or 2D (drop accumulations cuts of the spatio-temporal

field. Further investigations would be needed to establish a rigorous link between the full underlying process and these cuts. This would enable to improve our representation of the full 3+1D structure of the field with all its drops which is the ultimate goal. We showed that during heaviest rainfall period the commonly used Poisson hypothesis is not valid and results suggest that a framework relying on multifractals may help overcome some of current discrepancies. Finally it should be mentioned that this work has some strong consequences on the remote sensing of rainfall with weather radar for instance. Indeed radar rainfall retrieval algorithms usually assume that drops are homogeneously distributed within the scanned volume which is not necessarily the case especially during the most intense portions of rainfall events. This issue of non-uniform beam filling issue is experienced by radar analysts. Given the scale gap between the volume scanned by radar and the studied volume of the vertical column (at least a ratio of 10^6 between the volumes), it is difficult to be more affirmative, but it converges with studies of the speckle effect, due to coherent backscattering of inhomogeneously distributed drops, which underpinned strong biases in the rainfall rate estimates. Some theoretical investigations of this effect with the help of multifractals have already been carried out (Lovejoy et al. 1996, Schertzer et al. 2012), and further empirical analysis with the reconstructed columns could help to better quantify the actual consequences of this effect. The variability observed between consecutive snapshots of vertical columns (done every second in this paper) also suggests that the sampling uncertainty of radar data due to limited revisit time in the scanning strategies should be investigated more in depth. These two issues will be analysed in future work.

Acknowledgments

The authors greatly acknowledge partial financial support form the Chair “Hydrology for Resilient Cities” (sponsored by Veolia) of Ecole des Ponts ParisTech, EU NEW-INTERREG IV RainGain Project (www.raingain.eu), and EU Climate KIC Blue Green Dream project (www.bgd.org.uk). Tim Raupach is also acknowledged for having selected the studied events and providing Fig. 1.

References

Anselmet, F., Antonia, R.A., Danaila, L., 2001: Turbulent flows and intermittency in laboratory experiments. *Planet. Space Sci.*, **49**, 1177–1191.

Battaglia, A., Rustemeier, E., Tokay, A., Blahak, U. and Simmer, C., 2010: PARSIVEL Snow Observations: A Critical Assessment. *J. Atmos. Oceanic Technol.*, **27**(2), 333-344.

Cao, Q. et al., 2008: Analysis of Video Disdrometer and Polarimetric Radar Data to Characterize Rain Microphysics in Oklahoma. *J. Appl. Meteor. Climatol.*, **47**(8), 2238-2255.

Cotton, W.R. and Gokhale, N.R., 1967: Collision, coalescence, and breakup of large water drops in a vertical wind tunnel. *J. Geophys. Res.*, **72** (16), 4041–4049.

de Lima, M.I.P. and de Lima, J., 2009: Investigating the multifractality of point precipitation in the Madeira archipelago. *Nonlin. Processes Geophys.*, **16**(2), 299-311.

de Lima, M.I.P. and Grasman, J., 1999: Multifractal analysis of 15-min and daily rainfall from a semi-arid region in Portugal. *J. Hydrol.*, **220**(1-2), 1-11.

de Montera, L., Barthes, L., Mallet, C. and Gole, P., 2009: The Effect of Rain-No Rain Intermittency on the Estimation of the Universal Multifractals Model Parameters. *J. Hydrometeor.*, **10**(2), 493-506.

619Desaulnier-Soucy, N., Lovejoy, S. and Schertzer, D., 2001: The continuum limit in rain and
620 the HYDROP experiment. *J. Atm. Res.*, **59-60**, 163-197.
621Ducrocq et al., 2014: HyMeX-SOP1, the field campaign dedicated to heavy precipitation and
622 flash flooding in the northwestern Mediterranean. *Bull. Amer. Meteor. Soc.*, doi:
623 http://dx.doi.org/10.1175/BAMS-D-12-00244.1
624Fitton, G., Tchiguirinskaia, I., Schertzer, D., Lovejoy, S., 2011: Scaling Of Turbulence In The
625 Atmospheric Surface-Layer: Which Anisotropy?. *Journal of Physics: Conference*
626 *Series*, **318**, doi:10.1088/1742-6596/318/7/072008
627Fraedrich, K. and Larnder, C., 1993: Scaling regimes of composite rainfall time-series. *Tellus*
628 *Series a-Dynamic Meteorology and Oceanography*, **45A**(4), 289-298.
629Frasson, R. P. d. M., L. K. d. Cunha, and W. F. Krajewski (2011), Assessment of the Thies
630 optical disdrometer performance, *Atmos. Res.*, **101**, 237-255, doi:
631 10.1016/j.atmosres.2011.02.014.
632Gabella, M., Pavone, S., Perona, G., 2001: Errors in the estimate of the fractal correlation
633 dimension of raindrop spatial distribution. *J. Appl. Meteor.*, **40**, 664–668.
634Gires, A. et al., 2012: Quantifying the impact of small scale unmeasured rainfall variability on
635 urban runoff through multifractal downscaling: A case study. *J. Hydrol.*, **442-443**, 117-
636 128.
637Gires, A., Tchiguirinskaia, I., Schertzer, D. and Lovejoy, S., 2011: Analyses multifractales et
638 spatio-temporelles des precipitations du modele Meso-NH et des donnees radar.
639 *Hydrol. Sci. J.*, **56**(3), 380-396.
640Gires, A., Tchiguirinskaia, I., Schertzer, D. and Lovejoy, S., 2013: Development and analysis
641 of a simple model to represent the zero rainfall in a universal multifractal framework.
642 *Nonlin. Processes Geophys.*, **20**(3), 343-356.

643Gires, A. et al., 2014: Influence of small scale rainfall variability on standard comparison
644 tools between radar and rain gauge data. *Atmos. Res.*, **138**(0), 125-138.
645Hubert, P. et al., 1993: Multifractals and extreme rainfall events. *Geophys. Res. Lett.*, **20**, 931-
646 934.
647Jaffrain, J. and Berne, A., 2011. Experimental Quantification of the Sampling Uncertainty
648 Associated with Measurements from PARSIVEL Disdrometers. *J. Hydrometeor.*,
649 **12**(3): 352-370.
650Jameson, A.R. and Kostinski, A.B., 1998: Fluctuation Properties of Precipitation. Part II:
651 Reconsideration of the Meaning and Measurement of Raindrop Size Distributions. *J.*
652 *Atmos. Sci.*, **55**(2), 283-294.
653Jameson, A.R., Kostinski, A.B. and Kruger, A., 1999: Fluctuation Properties of Precipitation.
654 Part IV: Finescale Clustering of Drops in Variable Rain. *J. Atmos. Sci.*, **56(1)**, 82-91.
655Joss, J. and Waldvogel, A., 1967: Ein spektrograph fur nieder chlagstropfen mit automatischer
656 auswertung (A spectrograph for raindrops with automatic interpretation). *Pure Appl.*
657 *Geophys. Rev. A.*, **68**, 240-246.
658Kostinski, A.B. and Jameson, A.R., 1997: Fluctuation Properties of Precipitation. Part I: On
659 Deviations of Single-Size Drop Counts from the Poisson Distribution. *J. Atmos. Sci.*,
660 **54**(17), 2174-2186.
661Krajewski, W.F. et al., 2006: DEVEX-disdrometer evaluation experiment: Basic results and
662 implications for hydrologic studies. *Adv. Wat. Resour.*, **29**(2), 311-325.
663Kruger, A. and Krajewski, W.F., 2002: Two-Dimensional Video Disdrometer: A Description.
664 *J. Atmos. Oceanic Technol.*, **19(5)**, 602-617.
665Ladoy, P., Schmitt, F., Schertzer, D. and Lovejoy, S., 1993: The multifractal temporal
666 variability of Nimes rainfall data. *Comptes Rendus de l'Academie Des Sciences Serie*
667 *Ii*, **317**(6), 775-782.

668Lavergnat, J. and Golé, P., 1998: A Stochastic Raindrop Time Distribution Model. *J. Appl.*
669 *Meteor.*, **37**(8), 805-818.
670Lazarev, A., Schertzer, D., Lovejoy, S. and Chigirinskaya, Y., 1994: Unified multifractal
671 atmospheric dynamics tested in the tropics: part II, vertical scaling and Generalized
672 Scale Invariance. *Nonlin. Processes Geophys.*, **1**, 115-123.
673Lilley, M., Lovejoy, S., Desaulniers-Soucy, N. and Schertzer, D., 2006: Multifractal large
674 number of drops limit in rain. *J. Hydrol.*, **328**(1-2), 20-37.
675Lovejoy, S., Duncan, M.R. and Schertzer, D., 1996: Scalar multifractal radar observer's
676 problem. *J. Geophys. Res.*, **101**, 26479-26492.
677Lovejoy, S. and Schertzer, D., 1990: Fractals, raindrops and resolution dependence of rain
678 measurements. *J. Appl. Meteor.*, **29**(11), 1167-1170.
679Lovejoy, S. and Schertzer, D., 1995: Multifractals and rain. *New Uncertainty Concepts in*
680 *Hydrology and Hydrological modelling*, A.W. Kundzewicz, Ed., Cambridge Press, 62-
681 103.
682Lovejoy, S. and Schertzer, D., 2008: Turbulence, rain drops and the l**1/2 number density
683 law. *New J. of Physics*, **10**, 32pp.
684Lovejoy, S., Schertzer, D. and Allaire, V., 2008: The remarkable wide range spatial scaling of
685 TRMM precipitation. *J. Atmos. Research*, **90**, 10-32.
686Mandapaka, P.V., Lewandowski, P., Eichinger, W.E. and Krajewski, W.F., 2009: Multiscaling
687 analysis of high resolution space-time lidar-rainfall. *Nonlin. Processes Geophys.*,
688 **16**(5), 579-586.
689Nykanen, D.K. and Harris, D., 2003: Orographic influences on the multiscale statistical
690 properties of precipitation. *J. Geophys. Res.-Atm.*, **108**(D8),
691Olsson, J., 1995: Limits and characteristics of the multifractal behavior of a high-resolution
692 rainfall time series. *Nonlin. Processes Geophys.*, **2**, 23-29.

693Royer, J.-F., Biaou, A., Chauvin, F., Schertzer, D. and Lovejoy, S., 2008: Multifractal analysis
694 of the evolution of simulated precipitation over France in a climate scenario. *C.R.*
695 *Geoscience*, **340**, 431-440.
696Salles, C., Creutin, J.D. and Sempere-Torres, D., 1998: The optical spectropluviometer
697 revisited. *J. Atmos. Oceanic Technol.*, **15**(5), 1215-1222.
698Schertzer, D. and Lovejoy, S., 1987: Physical modelling and analysis of rain and clouds by
699 anisotropic scaling and multiplicative processes. *J. Geophys. Res.*, **92**(D8), 9693-9714.
700Schertzer, D. and Lovejoy, S., 1997: Universal multifractals do exist!: Comments. *J. Appl.*
701 *Meteor.*, **36**(9), 1296-1303.
702Schertzer D, Tchiguirinskaia I, Lovejoy S, Hubert P., 2010: No monsters, no miracles: in
703 nonlinear sciences hydrology is not an outlier! *Hydrol. Sci. J.*, **55**(6), 965-979.
704Schertzer, D. and Lovejoy, S., 2011: Multifractals, generalized scale invariance and
705 complexity in geophysics. *International Journal of Bifurcation and Chaos*, **21**(12),
706 3417-3456.
707Schertzer, D., Tchiguirinskaia, I. and Lovejoy, S., 2012: Getting higher resolution rainfall
708 estimates: X-band radar technology and multifractal drop distribution. *Proceedings of*
709 *the Weather Radar and Hydrology symposium held in Exeter, UK, April 2011*, IAHS
710 Publ. 351.
711Tchiguirinskaia, I., Salles, C., Hubert, P., Schertzer, D., Lovejoy, S., Creutin, J. D. &
712 Bendjoudi, H., 2003: Mulitfractal analysis of the OSP measured rain rates over time
713 scales from millisecond to day. *In: IUGG2003*, Sapporo
714Tessier, Y., Lovejoy, S., Hubert, P., Schertzer, D. and Pecknold, S., 1996: Multifractal analysis
715 and modeling of rainfall and river flows and scaling, causal transfer functions. *J.*
716 *Geophys. Res.-Atm.*, **101**(D21), 26427-26440.

717Tessier, Y., Lovejoy, S. and Schertzer, D., 1993: Universal Multifractals: theory and
718 observations for rain and clouds. *J. Appl. Meteor.*, **32**(2), 223-250.
719Thurai, M. and Bringi, V.N., 2005: Drop Axis Ratios from a 2D Video Disdrometer. *J. Atmos.*
720 *Oceanic Technol.*, **22**(7), 966-978.
721Thurai, M., Peterson, W.A., Tokay, A., Schutz, C. and Gatlin, P., 2011: Drop size distribution
722 comparisons between Parsivel and 2-D video disdrometers. *Adv. Geosci.*, **30**, 3-9.
723Tokay, A., Petersen, W.A., Gatlin, P. and Wingo, M., 2013: Comparison of Raindrop Size
724 Distribution Measurements by Collocated Disdrometers. . *J. Atmos. Oceanic Technol.*,
725 **30**(8), 1672-1690
726Uijlenhoet, R., Stricker, J.N.M., Torfs, P.J.J.F. and Creutin, J.D., 1999: Towards a stochastic
727 model of rainfall for radar hydrology: testing the Poisson homogeneity hypothesis.
728 *Physics and Chemistry of the Earth, Part B: Hydrology, Oceans and Atmosphere*,
729 **24**(6), 747-755.
730Verrier, S., de Montera, L., Barthes, L. and Mallet, C., 2010: Multifractal analysis of African
731monsoon rain fields, taking into account the zero rain-rate problem. *J. Hydrol.*, **389**(1-2), 111-
732120.

733

734

735**Figure caption list**

736

737Figure 1: Picture of the installed 2DVD in Le Pradel, Ardèche, France

738

739Figure 2: (a) Example of a reconstruction for a 26 cm vertical column; dimensions are in mm,
740drops have been coloured according to size and their diameter has been multiplied by 4 to
741improve visibility (b) Illustration of the 36 m x 11 cm x 11 cm reconstructed column divided

742into smaller boxes. (c) Vertical evolution of the LWC (in g.m^{-3}) within the vertical column for
743the reconstructed field (top in black) and simulated assuming homogenous distribution of
744drop positions (bottom in red) for an instant of the 09-24-2012 event. The horizontal axis
745corresponds to the box number (0: ground level, 8192: top of the reconstructed column).
746
747Figure 3: (a) Spectral analysis of the vertical column snapshots for 60 seconds starting on 24
748September 2012 02:17 UTC. (b) *TM* analysis of the same data (points) and the corresponding
749synthetic field-same drops (size and velocity) but their position is randomly (uniformly)
750assigned (solid, curved lines). The linear regressions (straight lines on the right side of the
751figure) are performed only for large scales, i.e. 0.5 – 36 m (c) Same as in (b) zoomed on the
752large scales (d) Spectral analysis of the corresponding synthetic field.
753
754Figure 4: Illustration of the absence of scaling in columns with too low number of drops. (a)
755Same as in Fig. 3.b but for 60 time steps starting at 02:23UTC. (b) Scatter plot of r^2 for q=1.5
756in the *TM* analysis vs. the average number of drops in the studied columns. (c) Scatter plot of
757the average number of drops in the studied columns vs. the indicative rain rate computed at
758ground level.
759
760Figure 5: Figures are plotted for the 09-24-2012 event (a) Temporal evolution of the number
761of drops passing through the sampling area with 1ms time steps. (b), (c) and (d) Temporal
762evolution of the rain rate during the same event with time steps of 1ms, 1s and 1min
763respectively. (e) Temporal evolution of the average mass weighted diameter. (f), (g) and (h):
764same as in (b), (c) and (d) expressed in $\log_\lambda$.
765

766Figure 6: Spectral analysis (a) and TM analysis (b) data corresponding to 140 min of the 10-
76723-2013 event with 1 ms time steps (time series of length 2^{23}).

768

769Figure 7: Top: natural drop accumulation: rain accumulation map (left) and occurrence map
770(right) for 150 consecutive drops during the 10-23-2013 event. Bottom: Same as Top but for a
771homogenised version of the drop accumulation (see text for details). The colour scale is in
772mm x 10^{-3}

773

774Figure 8: Fractal analysis (Eq. 1 in log-log plot) of the drop position for 10-23-2013 event
775with 150 drops per drop accumulation map (ensemble analysis on the 1179 pictures recorded
776on a total duration of 12h). (a) On the drop centres. (b) Considering all the pixels occluded by
777drops.

778

779Figure 9: (a) Duration need to record pictures with 350 drops during the 10-27-2013 event (b)
780The exceedance probability of the distribution of the durations in a log-log plot (Δt and x are
781in s).

782

783

784

785

786

787

788

789

790

Tables

Event	Approx duration (h)	Total depth (mm)	Maximum rain rate (mm/h)
09-24-2012	0.6	10.9	103
10-26-2012	20	20.4	45.9
10-23-2013	8	21.4	76.1
10-27-2013	6	10.6	76.9

Table 1: Basic features of the studied events

Event	Studied duration (min)	Large scale range (min)	α	C_1
09-24-2012	35	35 – 2	1.95	0.21
10-26-2012	140	140 – 9	1.7	0.3
10-23-2013	140	140 – 2	1.3	0.3
10-27-2013	140	140 – 2	1.03	0.47

Table 2: UM parameter estimates for large scales in the temporal analysis of 1 ms resolution time series for the 5 studied events.

Figure list:

Figure 1: Picture of the installed 2DVD in Le Pradel, Ardèche, France

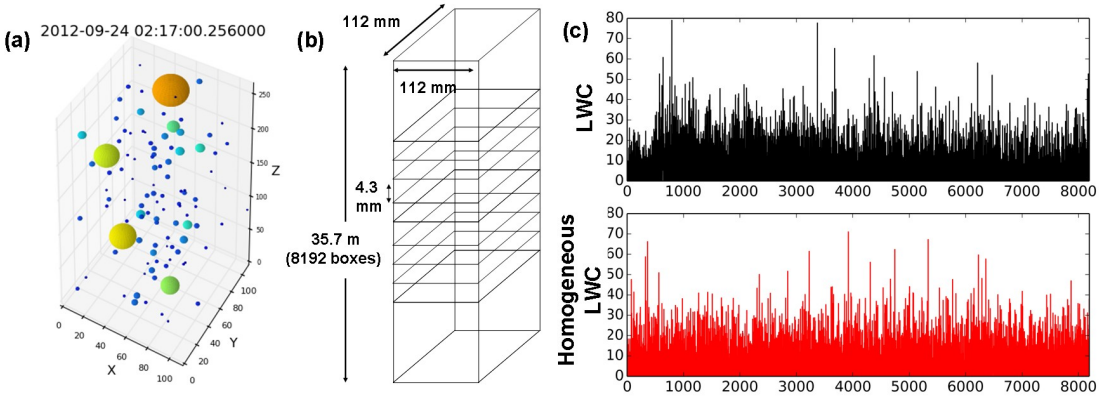

Figure 2: (a) Example of a reconstruction for a 26 cm vertical column; dimensions are in mm, drops have been coloured according to size and their diameter has been multiplied by 4 to improve visibility (b) Illustration of the 36 m x 11 cm x 11 cm reconstructed column divided into smaller boxes. (c) Vertical evolution of the LWC (in $g.m^{-3}$) within the vertical column for the reconstructed field (top in black) and simulated assuming homogenous distribution of drop positions (bottom in red) for an instant of the 09-24-2012 event. The horizontal axis corresponds to the box number (0: ground level, 8192: top of the reconstructed column).

34

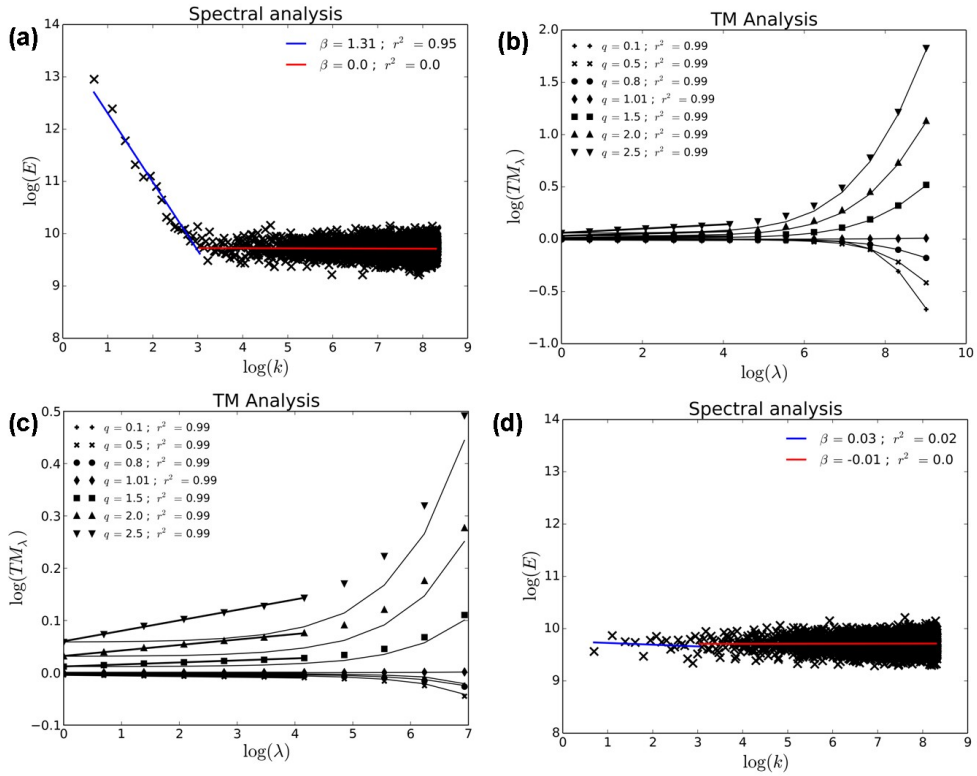

819

820Figure 3: (a) Spectral analysis of the vertical column snapshots for 60 seconds starting on 24

821September 2012 02:17 UTC. (b) *TM* analysis of the same data (points) and the corresponding

822synthetic field-same drops (size and velocity) but their position is randomly (uniformly)

823assigned (solid, curved lines). The linear regressions (straight lines on the right side of the

824figure) are performed only for large scales, i.e. 0.5 – 36 m (c) Same as in (b) zoomed on the

825large scales (d) Spectral analysis of the corresponding synthetic field.

826

827

828

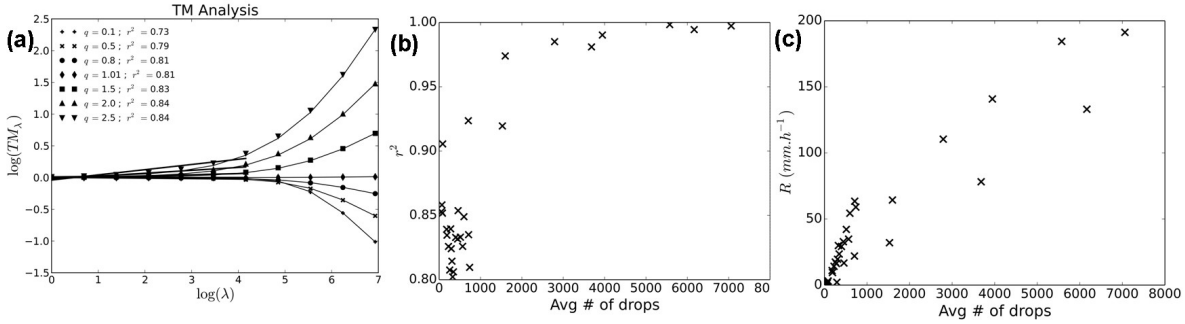

829

35

830Figure 4: Illustration of the absence of scaling in columns with too low number of drops. (a)
831Same as in Fig. 3.b but for 60 time steps starting at 02:23UTC. (b) Scatter plot of r^2 for q=1.5
832in the *TM* analysis vs. the average number of drops in the studied columns. (c) Scatter plot of
833the average number of drops in the studied columns vs. the indicative rain rate computed at
834ground level.

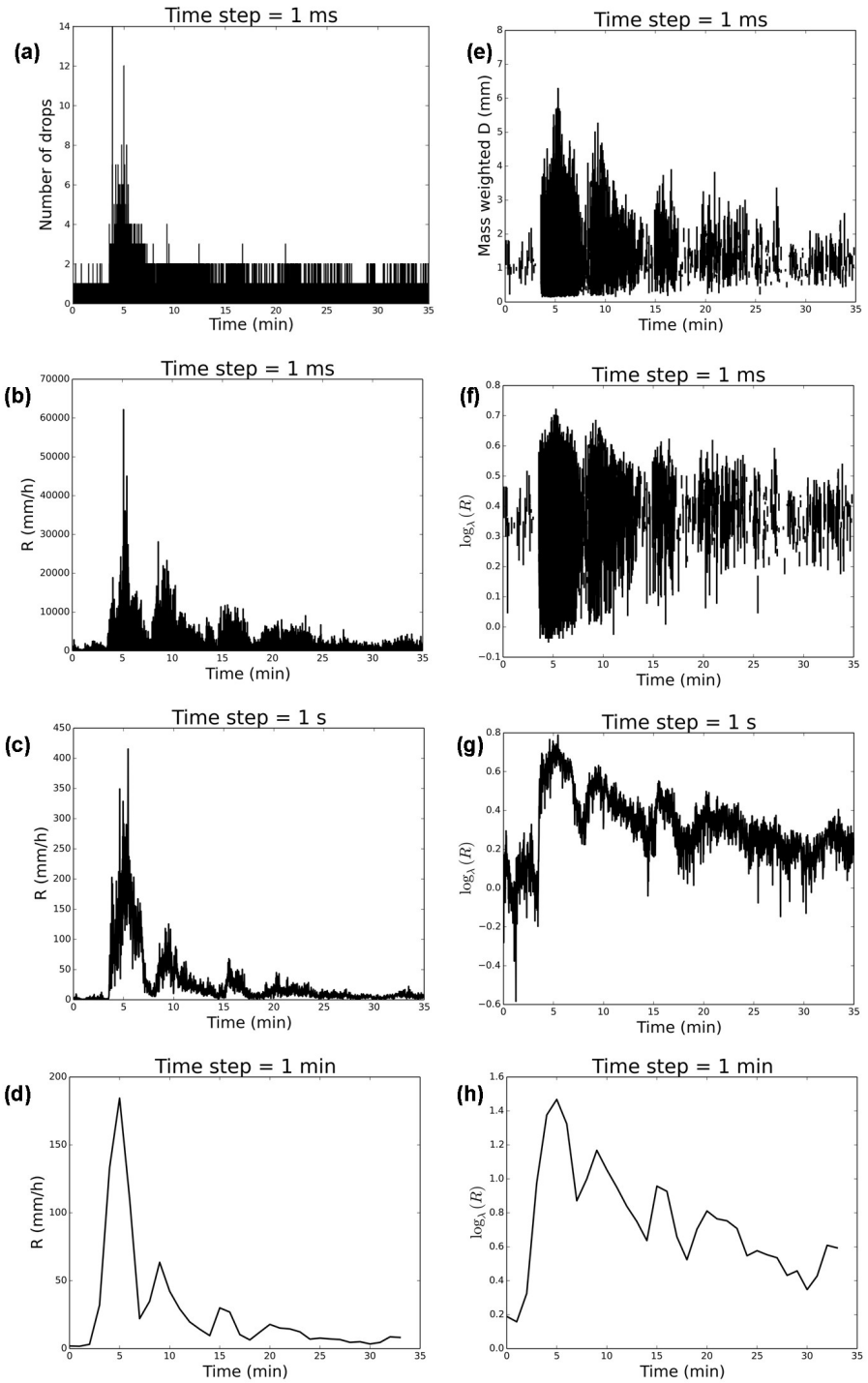

835

836

837

838Figure 5: Figures are plotted for the 09-24-2012 event (a) Temporal evolution of the number
839of drops passing through the sampling area with 1ms time steps. (b), (c) and (d) Temporal
840evolution of the rain rate during the same event with time steps of 1ms, 1s and 1min
841respectively. (e) Temporal evolution of the average mass weighted diameter. (f), (g) and (h):
842same as in (b), (c) and (d) expressed in $\log_\lambda$.

843

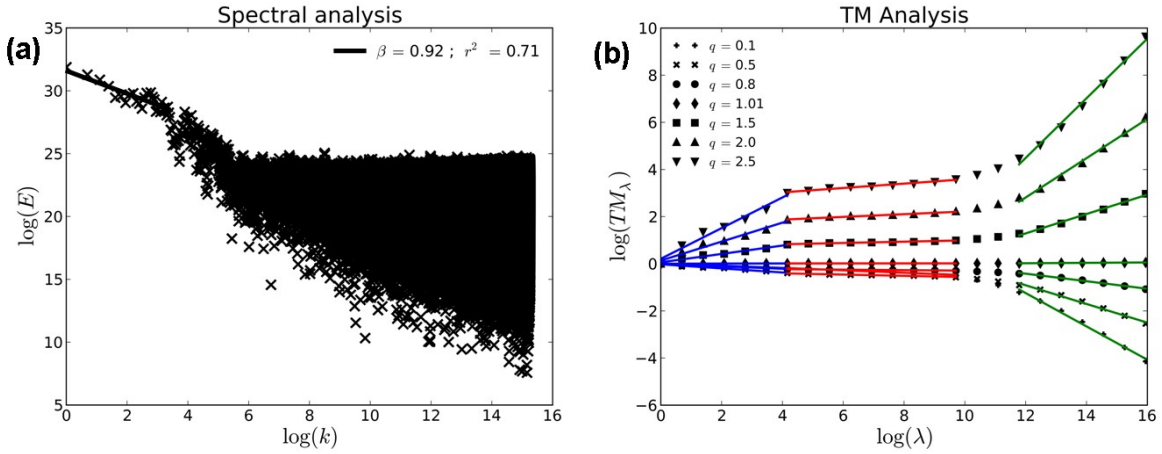

844

845Figure 6: Spectral analysis (a) and TM analysis (b) data corresponding to 140 min of the 10-
84623-2013 event with 1 ms time steps (time series of length 2^{23}).

847

848

37

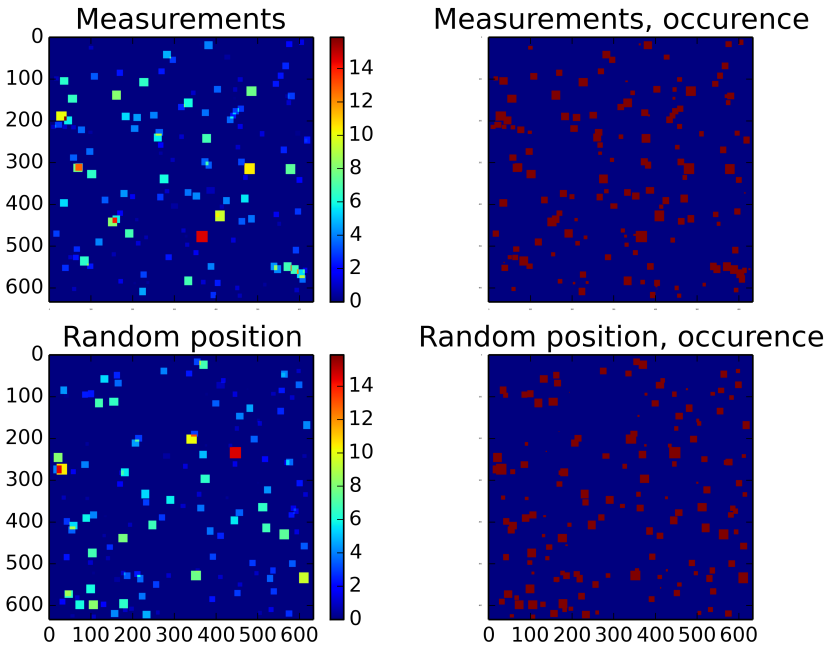

849

850Figure 7: Top: natural drop accumulation: rain accumulation map (left) and occurrence map

851(right) for 150 consecutive drops during the 10-23-2013 event. Bottom: Same as Top but for a

852homogenised version of the drop accumulation (see text for details). The colour scale is in

853mm x 10^{-3}

854

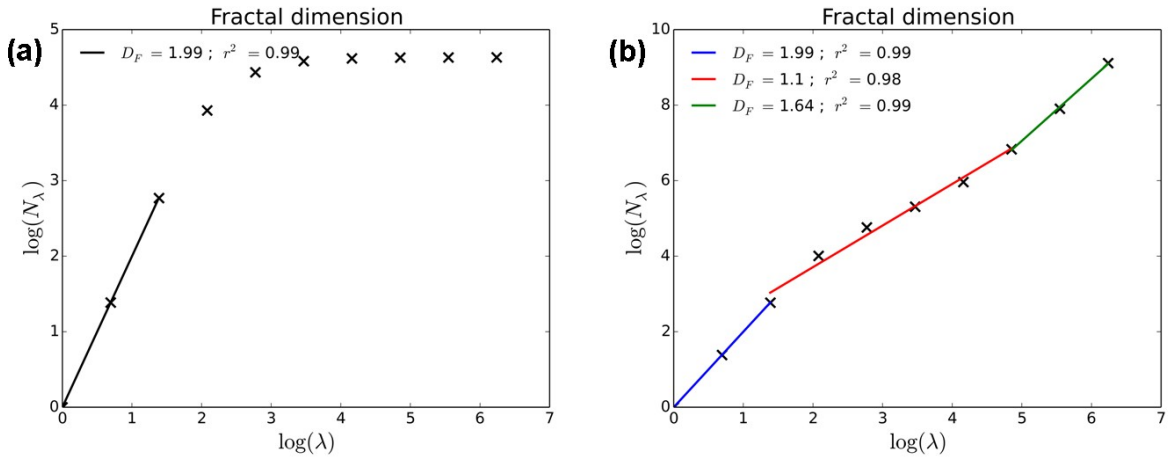

855

856Figure 8: Fractal analysis (Eq. 1 in log-log plot) of the drop position for 10-23-2013 event

857with 150 drops per drop accumulation map (ensemble analysis on the 1179 pictures recorded

858on a total duration of 12h). (a) On the drop centres. (b) Considering all the pixels occluded by

859drops.

38

860

861

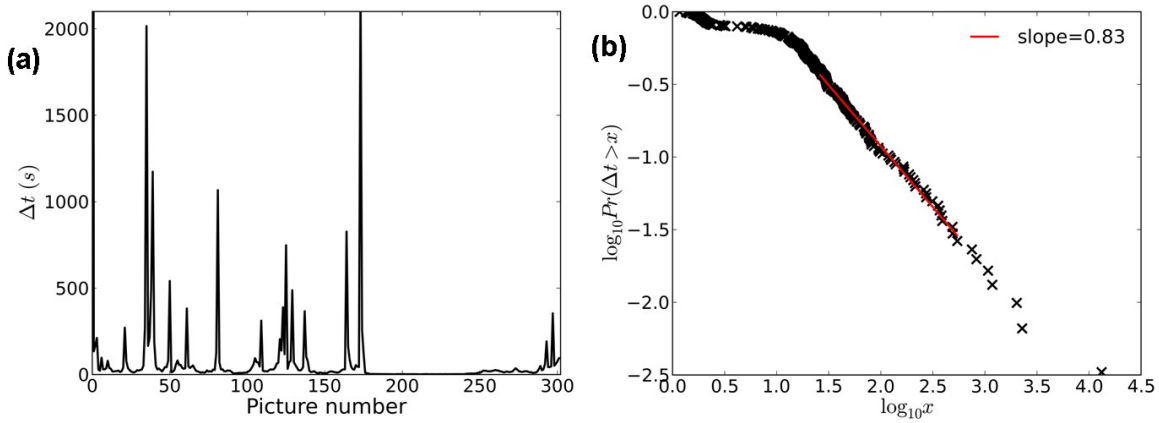

862

863Figure 9: (a) Duration need to record pictures with 350 drops during the 10-27-2013 event (b)

864The exceedance probability of the distribution of the durations in a log-log plot (Δt and x are

865in s).

866

39